remote sensing

MDPI

Article

A Model-Downscaling Method for Fine-Resolution LAI Estimation

Jingyu Zhang [1,2], Jindi Wang [1,2], Rui Sun [1,2], Hongmin Zhou [1,2,*] and Helin Zhang [1,2]

[1] State Key Laboratory of Remote Sensing Science,
Jointly Sponsored by Beijing Normal University and Institute of Remote Sensing and Digital Earth of Chinese Academy of Sciences, Beijing 100875, China; zjy@mail.bnu.edu.cn (J.Z.); wangjd@bnu.edu.cn (J.W.); sunrui@bnu.edu.cn (R.S.); 201931051035@bnu.edu.cn (H.Z.)

[2] Beijing Engineering Research Center for Global Land Remote Sensing Products,
Institute of Remote Sensing Science and Engineering, Faculty of Geographical Science,
Beijing Normal University, Beijing 100875, China

* Correspondence: zhouhm@bnu.edu.cn; Tel.: +86-010-5880-6011; Fax: +86-010-58805274

Received: 16 November 2020; Accepted: 17 December 2020; Published: 18 December 2020

Abstract: The leaf area index (LAI) is a critical parameter for characterizing the structure and function of vegetation in ecosystems. Currently, operational LAI products always have coarse spatial resolution, and fine-resolution LAI maps are urgently needed for ecological environment assessment and the precise monitoring of cropland growth. LAI downscaling methods are efficient at improving the spatial resolution of LAI products but often ignore the scaling effect of the model. In this study, a novel model-downscaling method is proposed for fine-resolution LAI estimation. It uses scaling equations of model parameters (SEMPs) to describe the scaling relations of models at different spatial resolutions and construct a downscaled model from a coarse-resolution model. Landsat Normalized Difference Vegetation Index (NDVI) at 30 m and Global LAnd Surface Satellite (GLASS) LAI at 1 km spatial resolutions are used because they are readily available. The downscaled model is evaluated by a fine-resolution model directly constructed with fine-resolution data. The fine-resolution LAI values estimated by this model-downscaling method are evaluated with field LAI measurements. The validation results show that the proposed method can generate highly accurate LAIs, with an RMSE of 0.821 at the Pshenichne cropland site in Ukraine and an RMSE of 0.515 at the Camerons forest site in Australia when compared with field LAI measurements. The results are also better than those of Ovakoglou's downscaling method. These results demonstrate that the model-downscaling method for fine-resolution LAI estimation is viable and referable for related studies.

Keywords: leaf area index; fine resolution; downscaling modeling; model parameters

1. Introduction

The leaf area index (LAI) is defined as half of the total green leaf area per unit ground horizontal surface area [1], which is a critical parameter that quantitatively describes the structure and function of vegetation [2]. LAI products (e.g., Moderate Resolution Imaging Spectroradiometer (MODIS) LAI, Global LAnd Surface Satellite (GLASS) LAI, the second version of global biophysical products (GEOV2) LAI, Visible Infrared Imaging Radiometer Suite (VIIRS) LAI and EUMESAT Polar System (EPS) LAI) with coarse resolutions are the critical input data for terrestrial ecosystem and land-surface models [3–9]. Fine-resolution LAI maps need to be applied in ecological environment assessments and the precise monitoring of cropland growth [10,11]. Coarse-resolution LAI products require upscaled fine-resolution LAI maps to verify their accuracy [12]. Achieving fine-resolution

LAI maps in a study area with limited ground measurement data requires downscaling coarse-resolution LAI products [13]. Downscaling refers to an increase in spatial resolution; upscaling refers to a decrease in spatial resolution [14]. Scaling plays an important role in the validation or application of the LAI. Open-access LAI products are mostly coarse-resolution products [3–9]. A downscaling method based on existing coarse-resolution LAI products could be a convenient and quick method to estimate fine-resolution LAI maps. Downscaling, which increases the information content, is more difficult than upscaling, which reduces the information content [15].

In the remote-sensing field, remote-sensing algorithms for LAI estimation are usually described as follows:

$$s = f(LAI, p) \tag{1}$$

where f takes observation data (s) to retrieve the *LAI*, and p is a set of model parameters. According to Equation (1), we can study LAI scaling from three aspects: observation data (s), models (f) and land surface parameter products (LAI).

Research on LAI upscaling has mostly focused on land surface parameter products [16–21]. For example, Chen assumed that the scaling effect was due to solely considering the dominant surface types while ignoring other types and proposed a method in which the pixel value is the weighted sum of the subpixel LAI considering the surface type of the subpixel [16]. However, the subpixel contained other types, the fraction of the cover type was changed with spatial resolutions [22], and this method ignored the scaling effect of the model. If a model f_{fine} is established at a fine resolution and is directly applied to a coarse resolution, the equation is:

$$S_{coarse} = f_{fine}(LAI_{coarse}, p_{fine}) \tag{2}$$

where S_{coarse} is the observation vector at the coarse resolution, LAI_{coarse} is the target parameter at the coarse resolution and p_{fine} is a set of parameters in the model f_{fine}. The spatial resolutions of the observation data and the model are inconsistent in Equation (2). Other research has considered the scaling effect of the model. Studies have applied Taylor's theorem (TT) [22], the wavelet-fractal technique (WF) [23] and fractal theory (FT) [24] to correct the scaling bias of LAI values.

In addition, several studies have examined LAI downscaling from the perspective of remote-sensing models. The main concept was to construct models with coarse resolution data that are achieved in homogeneous pixels, and these models were used to estimate fine-resolution LAI maps. For example, Gao et al. developed a regression tree between homogeneous and high-quality MODIS LAI data and pixel-aggregated Landsat surface reflectance for fine-resolution LAI estimation [25,26]. Moreover, Landsat LAI values were estimated using MODIS regression equations and Landsat Enhanced Vegetation Index (EVI) values [27]. In an LAI downscaling study, these methods ignored the scaling effect of the remote-sensing model. The fraction of the cover type was changed with spatial resolution [22]. Usually, the homogeneous area at a coarse resolution is heterogeneous at a fine resolution when measured by the surface types. When assessing remote-sensing algorithms, several studies have considered the scaling effect of the model. The main concept was to construct a model at a specific spatial resolution or to build a scale-invariant model [28,29]; the former was more popular (e.g., a model of leaf optical properties spectra (PROSPECT) established at the leaf scale [30] and the geometric optical model constructed at the canopy scale [31]). However, there is little research on model scaling, and there is little research on LAI downscaling from the perspective of a model-downscaling method.

The spatial heterogeneity of the land surface and the nonlinearity of remote-sensing models are commonly considered to be the causes of scaling effects [18,19,32]. The spatial heterogeneity of the land surface is the fundamental cause of scale issues in remote-sensing [21,33] because it is an intrinsic property. The degree of spatial heterogeneity changes with spatial resolution [28]. Models are mathematical expressions used to characterize land surfaces, and a model that is established at a spatial resolution records the information at that spatial resolution. A remote-sensing model can hardly be scale-invariant [34]. Therefore, studying the scaling relation of models that are established

at disparate spatial resolutions would be a breakthrough for LAI downscaling. Is there an existing scaling relation for models? How can model scaling be realized to make a model consistent with the observation data at the spatial resolution? These are the issues we attempt to address in this paper.

In this paper, a novel LAI downscaling method is proposed from the perspective of model downscaling by considering the scaling effect of the model. The results of this study demonstrate that the scaling relation of models at different spatial resolutions can be expressed by scaling equations of model parameters (SEMPs) according to preliminary research. With SEMPs, the downscaled model can be built with high accuracy. The fine-resolution LAI estimated by this model-downscaling method meets the accuracy requirements of applications. The model-downscaling method proposed in this paper is effective and viable.

2. Materials

2.1. Field LAI

Many institutions have carried out the verification and validation of remotely sensed LAI products and have accumulated some ground observation data. Among them, we collected data from the VAlidation of Land European Remote-Sensing Instruments (VALERI) project (http://w3.avignon.inra.fr/valeri/) and the ImagineS project (http://www.fp7-imagines.eu/) because they contain a relatively large number of field measurements suitable for building statistical models [35]. Additionally, we collected basic information for each collected site. The VALERI project is hosted by the Centre National d'Etudes Spatiales (CNES) and has established a global site network. This project provides fine-resolution LAI maps that are created from ground measurements to validate products that are derived from satellite observations. The ImagineS project has implemented campaigns since 2013 to validate satellite-derived biophysical products and provides field LAI and fine-resolution LAI maps.

In this study, the selected sites contained the following four characteristics. First, the coordinates for the ground sampling points could be obtained to extract the surface reflectance, which is consistent with the location of the ground measurements. Second, the dates of the ground observations could be obtained to ensure that the downloaded remotely sensed surface reflectance images are from the same period. Third, the sites provide the land cover types for cropland and forest model constructions. Finally, the sites clarify whether the LAI is true or effective for future use.

In the ImagineS project, the data provided on the website include the true LAI. In the VALERI project, most of the data are the effective LAI, and we can convert them into a true LAI by Equation (3):

$$LAI_t = LAI_{eff} / \Omega \quad (3)$$

where Ω is the clumping index (CI), which describes the distribution of leaves in the vegetation canopy. LAI_t represents the true LAI, and LAI_{eff} represents the effective LAI. The CI we used was expanded by new and complete year-round observations from POLDER 3 and was terrain-effect corrected [36]. Then, a quality control check of these data was conducted; the data preprocessing procedure consists of four steps: first, the field LAI measurements, whose values were lower than 0.1 were excluded, because when ground LAI values are lower than 0.1, the Normalized Difference Vegetation Index (NDVI) values are related to the background of soil, litter and so on, and the uncertainty of these NDVI values is large [37]; second, for a given site, the land cover types with proportions of samples less than 1% of the overall dataset were eliminated; third, the exceptional data were identified, and auxiliary data were used to recheck them to determine whether they were used. Fourth, sites with relatively large numbers of field LAI measurements were chosen. In total, we screened 14 sites from the two projects to build a basic research database; 6 sites were covered by cropland and 8 sites by forest. The basic information of these sites is shown in Table 1 and includes the following: the site name, country, location, day of the year (DOY), year, land cover type, instrument for the LAI measurements and the number of ground samples. Generally, field LAI measurements are regarded as the reference values of fine-resolution LAI products [38].

Table 1. Information on the selected sites in the basic research database.

ID	Site Name	Country	Location	DOY	Year	Land Cover	Instrument	Number of Ground Samples
1	Camerons	Australia	32.598°S 116.254°E	61–64	2004	Broadleaf forest	DHP	29
2	Concépcion	Chile	37.467°S 73.470°W	7–10	2003	Coniferous forest	DHP	26
3	Gnangara	Australia	31.534°S 115.882°E	58–63	2004	Broadleaf forest	DHP	31
4	Hirskangas	Finland	62.643°N 27.011°E	219–232	2003	Coniferous forest	LAI-2000	30
5	Hyytiälä	Finland	61.851°N 24.308°E	170–206	2008	Coniferous forest	DHP	41
6	Larose	Canada	45.380°N 75.217°W	217–220	2003	Mixed forest	DHP	28
7	Puéchabon	France	43.725°N 3.652°E	162–166	2001	Broadleaf forest	DHP	60
8	Sierra Chincua	Mexico	19.675°N 100.282°W	345–347	2001	Coniferous forest	DHP	17
9	SouthWest	France	43.504°N 1.171°E	170–177 205–210 228–232 245–249	2013	Mixed cropland	DHP	71
10	Ottawa	Canada	45.035°N 75.767°W	153 178 186	2014	Mixed cropland	SDP/DHP	13
11	Pshenichne	Ukraine	50.077°N 30.232°E	134–137 163 212 174 204	2013 2014 2014 2015 2015	Mixed cropland	DHP	148
12	Barrax	Spain	39.054°N 2.101°W	139–140 147 203	2014 2015 2015	Mixed cropland	DHP/ LAI-2200	72
13	AHSPECT	France	43.573°N 1.375°E	173–176	2015	Mixed cropland	DHP/ LAI-2200/ Lp80	77
14	Capitanata	Italy	41.464°N 15.487°E	76 113	2015	Wheat	LAI-2000	182

SDP = Standard digital photography, DHP = Digital hemispherical photos.

2.2. Satellite Imageries

In this study, we used 30 m and 1 km spatial resolution NDVI and LAI data. The fine-resolution NDVI data were calculated from the Landsat Thematic Mapper (TM), Enhanced Thematic Mapper Plus (ETM+) or Operational Land Imager (OLI) surface reflectance images, and the spatial resolution was 30 m; the coarse-resolution NDVI data were obtained from the MOD13A2 product; the spatial resolution was 1 km, and the temporal resolution was 16 days. Xiao et al. (2014) generated the Global LAnd Surface Satellite (GLASS) LAI product [6], which is highly accurate and has been widely accepted [9]; therefore, we took the GLASS LAI value as the reference value of the LAI at the 1 km spatial resolution. The GLASS LAI is the true LAI, and the temporal resolution was 8 days. The projections and spatial resolutions of the GLASS LAI and MOD13A2 NDVI products were the same. The satellite imagery information we used in this paper is listed in Table 2 and includes the site name, acquired year, acquired date of the year (DOY), imagery type and number of ground samples. Because of the scattered observation times at the collection sites, Landsat 5 TM, Landsat 7 ETM+and Landsat 8 OLI data were used in this paper.

Table 2. The satellite imagery information used in this paper.

Site Name	Year	MOD13A2 NDVI (DOY)	GLASS LAI		Landsat NDVI	
			DOY	Number of Ground Samples	DOY	Satellite
Camerons	2004	049	057	20	62	TM
Concépcion	2003	001	009	20	10	ETM+
Gnangara	2004	049	057	12	62	TM
Hirskangas	2003	225	225	9	231	TM
Hyytiälä	2008	177	177	12	212	ETM+
Larose	2003	209	217	12	212	ETM+
Puéchabon	2001	161	161	12	177	ETM+
Sierra Chincua	2001	345	337	12	330	TM
SouthWest	2013	161	161	560	177	OLI
	2013	193	193		193	OLI
	2013	225	225		232	OLI
	2013	241	241		248	OLI
Ottawa	2014	145	145	12	153	OLI
		177	177		178	OLI
		177	185		186	ETM+
Pshenichne	2013	129	129	2000	138	OLI
	2014	161	161		157	OLI
	2014	209	209		212	OLI
	2015	161	161		176	OLI
	2015	193	193		189	OLI
Barrax	2014	129	129	36	130	OLI
	2015	145	145		126	OLI
	2015	193	193		197	OLI
AHSPECT	2015	161	161	16	174	OLI
Capitanata	2015	113	113	24	120	OLI
	2015	65	73		80	ETM+

For each site, two (LAI, NDVI) datasets with spatial resolutions of 1 km and 30 m were obtained. The coarse-resolution (LAI, NDVI) dataset was obtained from the GLASS LAI and MOD13A2 NDVI products, and the fine-resolution (LAI, NDVI) dataset was obtained from the ground LAI measurements of the VALERI or ImagineS projects and Landsat TM, ETM+ or OLI land surface reflectance products.

2.3. Validation Data

We chose the Pshenichne site (Figure 1a), which is covered by mixed cropland, and the Camerons site (Figure 1b), which is covered by forest, as the validation sites. The Pshenichne site in Ukraine covers a larger region than the other sites and has conducted five field campaigns, which means that this site has a large amount of coarse-resolution and fine-resolution data. This is significant for model establishment and LAI validation. The Camerons site in Australia has more coarse-resolution data to establish a statistical model, and the amount of ground LAI data is relatively large. Therefore, we chose it to validate the model-downscaling method in forests.

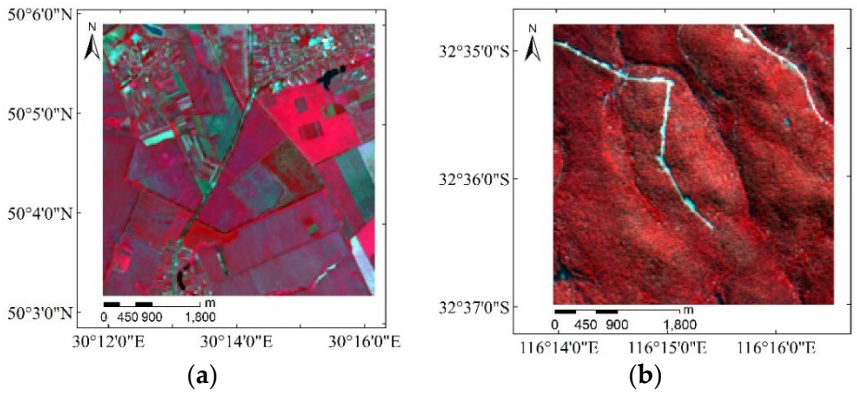

Figure 1. Location and study area of the validation site: (**a**) Pshenichne site (Landsat 8 NIR, Red and Green); (**b**) Camerons site (Satellite Pour L'observation de la Terre (SPOT) 4 NIR, Red and Green).

3. Method

We propose a model-downscaling method for fine-resolution LAI estimation in this section. For an invariant model form, the difference between models at different spatial resolutions is the model parameters, so model scaling is based on the scaling equations of model parameters (SEMPs). In the remote-sensing field, models for LAI estimation can be divided into three broad categories: statistical models, physical models and data-driven models [6]. Statistical models estimate the fine-resolution LAI by establishing a statistical relationship between the vegetation index (VI) and ground-based LAI measurements, and statistical models with a few variables are easy to operate [35,36]. Therefore, we chose a form of the NDVI-LAI statistical model for this research. Moreover, 30 m and 1 km spatial resolution data were used to study this issue because of their easy availability. The implementation of this method was divided into three steps, and the flowchart is shown in Figure 2.

Step 1: Construct the scaling equations of model parameters. The NDVI-LAI statistical models at 30 m spatial resolutions ($f(p)$) and the NDVI-LAI models at 1 km spatial resolutions ($F(P)$) were constructed. Then, we analyzed the scaling relation of model parameters at the two spatial resolutions, and SEMPs were constructed by linear regression for cropland sites and forest sites.

Step 2: In a validation site, the downscaled NDVI-LAI statistical model $f(p_{SD})$ was established with SEMPs and $F(P)$ at this site, which is suitable for fine-resolution LAI estimation. The downscaled model $f(p_{SD})$ was evaluated by the model $f(p)$ at this site.

Step 3: In the validation site, Landsat NDVIs were input into the downscaled model $f(p_{SD})$ to estimate the fine-resolution LAI. The fine-resolution LAI estimated by this model-downscaling method was evaluated by the field LAI and reference LAI maps.

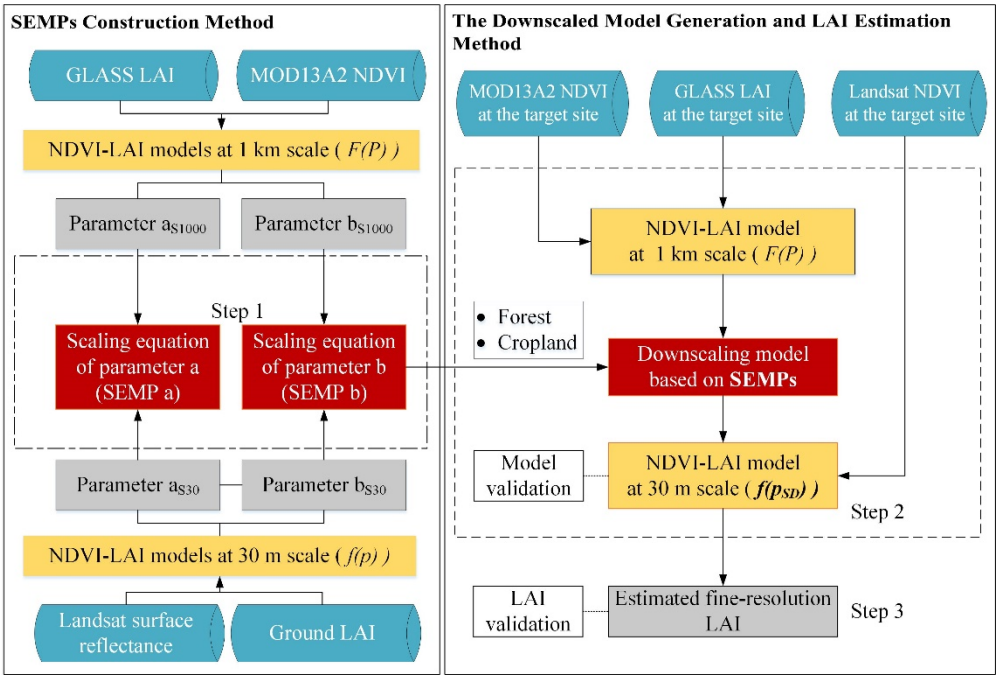

Figure 2. Flowchart of a model-downscaling methodology based on scaling equations of model parameters for fine-resolution leaf area index (LAI) estimation.

3.1. SEMP Construction Method

The scaling equations of model parameters (SEMPs) are established in this section. First, for the given model form, NDVI-LAI statistical models were established at 30 m and 1 km spatial resolutions. Each site listed in the basic research database (Table 1) constructed a model at a 1 km spatial resolution using MOD13A2 NDVI and GLASS LAI data and built a model at a 30 m spatial resolution using Landsat NDVI data and field LAI measurements. The NDVI-LAI statistical models were constructed by the ordinary least squares (OLS) method. Then, a SEMP was constructed for each

model parameter by the OLS method. The regression function for SEMP establishment was linear. The regression analysis was performed in MATLAB.

3.1.1. NDVI-LAI Model Construction

In the process of NDVI-LAI statistical model construction, the model form used is shown in Equation (4):

$$NDVI = \mathrm{a}LAI^{\mathrm{b}} \tag{4}$$

A simple form is preferred under the condition of ensuring model accuracy so that we can focus on the scaling relation of models. According to Equation (4), the NDVI-LAI model built at a spatial resolution of 30 m is expressed as Equation (5) and labeled as $f(p)$:

$$NDVI_{S30} = a_{S30} LAI_{S30}^{\ b_{S30}} \tag{5}$$

where parameter a_{S30} and parameter b_{S30} represent parameter a and parameter b of the model $f(p)$, the $NDVI_{S30}$ data are derived from the Landsat surface reflectance products in which a pixel records the land surface information with 30 m spatial resolution. The ground LAIs LAI_{S30} are also acquired at 30 × 30 m samples (some are at 20 × 20 m or 10 × 10 m samples). The spatial resolution of $NDVI_{S30}$ is consistent with the spatial resolution of LAI_{S30}, so $f(p)$ is suitable for 30 m LAI estimation. According to Equation (4), the NDVI-LAI model built at a spatial resolution of 1 km is expressed as Equation (6) and labeled as $F(P)$:

$$NDVI_{S1000} = a_{S1000} LAI_{S1000}^{\ b_{S1000}} \tag{6}$$

where a_{S1000} and b_{S1000} represent parameter a and parameter b of the model built at a 1 km spatial resolution. The $NDVI_{S1000}$ data are derived from the MOD13A2 NDVI products in which a pixel records the land surface information at a 1 km spatial resolution. The coarse-resolution LAIs LAI_{S1000} are derived from the GLASS LAI products. The spatial resolution of $NDVI_{S1000}$ is consistent with the spatial resolution of LAI_{S1000}, so $F(P)$ is the model suitable for 1 km LAI estimation. $F(P)$ and $f(p)$ models are constructed by the OLS method at the selected sites (Table 1).

To evaluate the accuracy of the NDVI-LAI models, R^2 was used, and the formula is as follows:

$$R^2 = \frac{\sum_{i=1}^{n} (y_i - \hat{y}_i)^2}{\sum_{i=1}^{n} (y_i - \overline{y})^2} \tag{7}$$

where y_i represents the observation values of NDVIs, $\hat{y}_i$ represents the estimated NDVIs, $\overline{y}$ represents the mean value of the NDVI observations and n represents the number of ground samples. The larger R^2 is, the higher the proportion of data that can be interpreted by the variables, and the more reliable the model is. Both the 30 m and 1 km NDVI-LAI statistical models used R^2 to evaluate the model accuracy.

3.1.2. SEMP Generation

The LAI was used to describe the vegetation canopy, and the VI was correlated with the physical properties of the vegetated canopy [39,40]. Therefore, the relationship between the LAI and NDVI (the NDVI-LAI model) is related to the vegetation canopy. Several studies have proven that there are strong relationships between the LAI and NDVI [41]. The NDVI is the most stable vegetation index for LAI estimation [42]. The NDVI-LAI model built by the observation data and the LAI values acquired at a specific spatial resolution records the information at that spatial resolution.

In this section, for an invariant statistical model form of the NDVI and LAI, scaling equations of model parameters (SEMPs) are established between the 30 m spatial resolution and the 1 km spatial resolution. To create the SEMPs, we first extracted parameter datasets from models $F(P)$ and $f(p)$. In Equation (4), the model parameters a and b affect the relation between the NDVI and LAI. The parameter a dataset consists of parameters a_{S1000} and parameters a_{S30}, which are extracted from $F(P)$ and $f(p)$ models in Section 3.1.1, and the parameter b dataset consists of parameters b_{S1000} and parameters b_{S30}, which are also extracted from $F(P)$ and $f(p)$ models in Section 3.1.1. Then, the SEMPs were built with linear function g. SEMP a and SEMP b are shown in Equations (8) and (9):

$$a_{S30} = g\left(T_a, a_{S1000}\right) \tag{8}$$

$$b_{S30} = g\left(T_b, b_{S1000}\right) \tag{9}$$

where T_a are parameters of SEMP a used to realize downscaling parameter a and T_b represents parameters of SEMP b used to complete downscaling parameter b. In Equations (8) and (9), a_{S30}, b_{S30}, a_{S1000} and b_{S1000} are variables. The OLS method was used to calculate T_a and T_b.

To evaluate the accuracy of the SEMPs, R^2 was used, as shown in Equation (10):

$$R^2 = \frac{\sum_{i=1}^{n}(y_i - \hat{y}_i)^2}{\sum_{i=1}^{n}(y_i - \overline{y})^2} \tag{10}$$

where y_i represents the true values of the model parameter, $\hat{y}_i$ represents the estimated values of the model parameter, $\overline{y}$ represents the mean of the true values and n represents the number of sites. The larger R^2 is, the higher the proportion of data that can be interpreted by the variables and the better the simulation results. During this process, we found that the accuracy of the SEMPs can be improved when we consider the land cover type. Therefore, we established the SEMPs for cropland and forest.

3.2. Model Downscaling Based on SEMPs

The GLASS LAI and MOD13A2 NDVI were used to construct the downscaled model $f(p_{SD})$ based on SEMPs. In a validation site, the NDVI-LAI statistical model $F(P)$, which was built with the MODIS NDVI and GLASS LAI data, recorded the vegetation information at a 1 km spatial resolution. To improve the accuracy of the 30 m LAI estimation, model $F(P)$ was downscaled to model $f(p_{SD})$. In this paper, the model $F(P)$ was downscaled based on SEMPs in Section 3.1, and $f(p_{SD})$ is shown as follows:

$$NDVI_{S30} = g(T_a, a_{s1000}) LAI_{S30}^{\,g(T_b, b_{S1000})} \tag{11}$$

During the process, a_{S1000} is converted into a_{S30} by SEMP a (Equation (8)), and b_{S1000} is converted into b_{S30} by SEMP b (Equation (9)). $f(p_{SD})$ is suitable for 30 m LAI estimation at the validation site. Thus far, model downscaling has been completed. SEMPs can transform the model from a 1 km spatial resolution to 30 m spatial resolution or from a 30 m spatial resolution to 1 km spatial resolution. In this paper, SEMPs were used for downscaling a model at a 1 km spatial resolution to a model that is suitable for a 30 m spatial resolution. The SEMPs can also be extended to other vegetation types and physical models. To compare the $NDVI_{f(p_{SD})}$ calculated by the model

$f(p_{SD})$ with the $NDVI_{f(P)}$ calculated by the model $f(p)$ to evaluate the accuracy of the downscaled NDVI-LAI statistical model, the equation is:

$$\frac{NDVI_{f(p_{SD})}}{NDVI_{f(P)}} = \frac{g(T_a, a_{s1000})LAI_{S30}^{\,g(T_b, b_{S1000})}}{a_{S30}LAI_{S30}^{\,b_{S30}}} \quad (12)$$

3.3. Fine-Resolution LAI Estimation

Landsat NDVIs at the validation site were input into the downscaled model $f(p_{SD})$, and the LAI with the 30 m spatial resolution was estimated. Usually, the process of fine-resolution LAI estimation is conducted by inputting fine-resolution NDVIs into the fine-resolution model, which is built by fine-resolution NDVIs and field LAIs. In areas where there is no field LAI or insufficient field LAI data, the fine-resolution model cannot be built. Downscaling the coarse-resolution model into a fine-resolution model is a new method for downscaling LAIs from the perspective of the remote-sensing model.

The fine-resolution LAI based on the model-downscaling method was compared with the reference LAI (field LAI measurements and the LAI maps obtained from field LAI) to evaluate the accuracy of this method. Moreover, Ovakoglou's downscaling method [27] was compared to evaluate this model-downscaling method.

4. Results

4.1. Accuracy of NDVI-LAI Statistical Models

NDVI-LAI statistical models of the 14 sites are built at 30 m and 1 km spatial resolutions. The models of the six cropland sites are shown in Figure 3, and the models of the eight forest sites are shown in Figure 4.

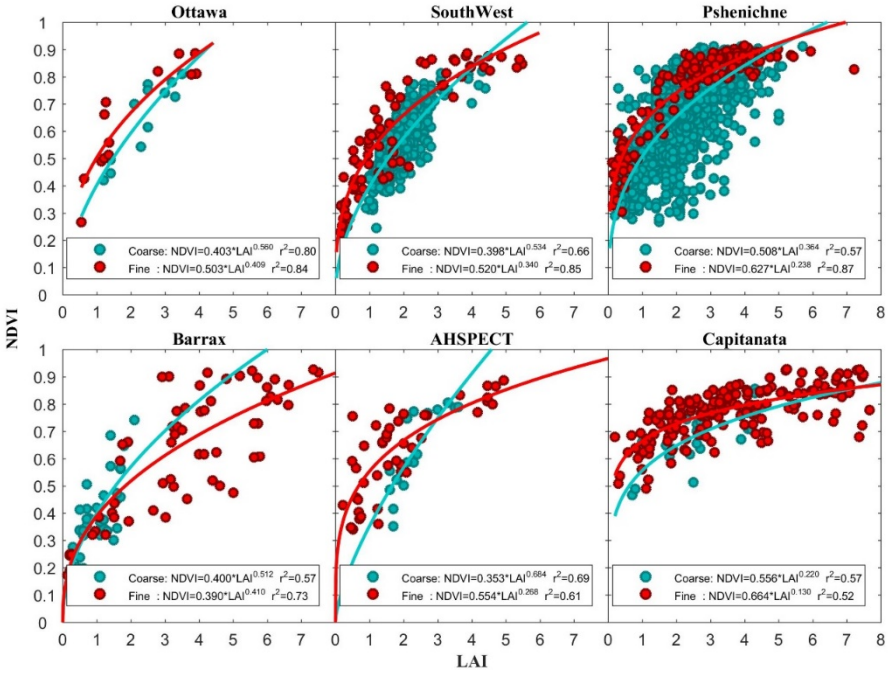

Figure 3. Normalized Difference Vegetation Index (NDVI)-LAI statistical models of the 6 cropland sites. The red points represent the (LAI, NDVI) dataset with 30 m spatial resolution, the red curves represent the model $f(p)$ at 30 m spatial resolution, the aquamarine points represent the (LAI, NDVI) dataset with 1 km spatial resolution and the aquamarine curves represent the model $F(P)$ at 1 km spatial resolution.

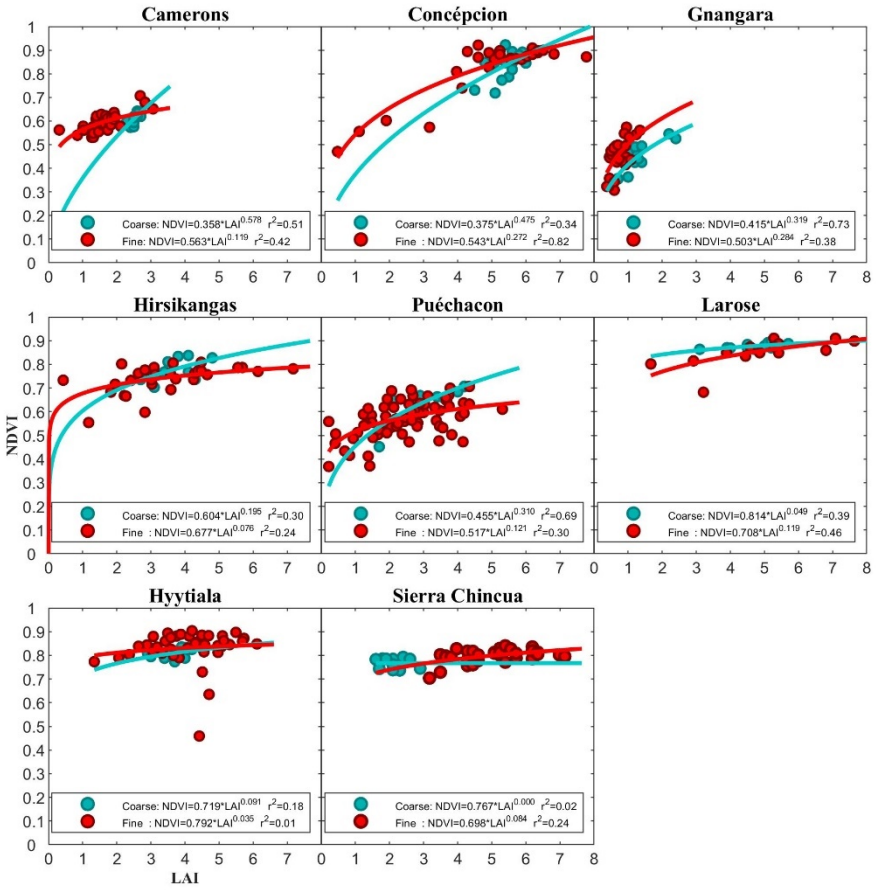

Figure 4. NDVI-LAI statistical models of the 8 forest sites. The red points represent the (LAI, NDVI) dataset with 30 m spatial resolution, the red curves represent the model $f(p)$ at 30 m spatial resolution, the aquamarine points represent the (LAI, NDVI) dataset with 1 km spatial resolution and the aquamarine curves represent the model $F(P)$ at 1 km spatial resolution.

In Figure 3, the cropland sites have high R^2 values (0.52–0.87) for both models at the 30 m and 1 km spatial resolutions, and these (LAI, NDVI) datasets are well described by these models. In the cropland sites, the curves of the models at the two spatial resolutions show the following characteristics: $f(p)$ is above $F(P)$ for smaller LAI values, and $f(p)$ is below $F(P)$ for larger LAI values.

In Figure 4, the first six forest sites have relatively high R^2 values (0.24–0.82) at both 30 m and 1 km spatial resolutions. These forest sites have lower R^2 values than the cropland sites. The Hyytiälä site has a low R^2 at the fine resolution because it has three outliers, but we have no reason to eliminate them. The Sierra Chincua site has a low R^2 at coarse resolution because the data are concentrated. Trees change slightly over one year—most sites only have field data for one year, and the samples are limited, so the model accuracy in forests is low. Except for the Sierra Chincua site and Larose site, other sites have the same curve tendency and characteristics as the cropland sites.

Altogether, Figures 3 and 4 indicate that the NDVI-LAI statistical models established at 30 m spatial resolutions are different from the NDVI-LAI statistical models established at 1 km spatial resolutions, and the traits are similar.

4.2. Accuracy of the Scaling Equations of Model Parameters

In the six cropland sites, the established SEMP a and SEMP b are shown in Figure 5a,b, respectively. In the eight forest sites, SEMP a and SEMP b are also established, and the results are shown in Figure 5c,d, respectively.

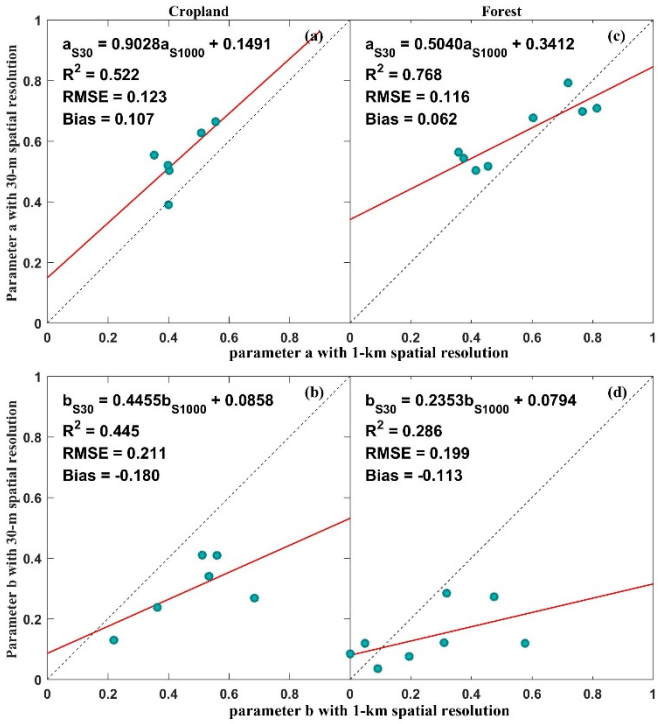

Figure 5. Scaling equations of model parameters (SEMPs); (**a**) SEMP a of the cropland sites; (**b**) SEMP b of the cropland sites; (**c**) SEMP a of the forest sites; (**d**) SEMP b of the forest sites.

Figure 5a shows the SEMP a of the cropland sites (Equation (13)):

$$a_{S30} = 0.9028 \times a_{S1000} + 0.1491 \quad (13)$$

where a_{S30} represents the parameter a in the 30 m spatial resolution model, a_{S1000} represents the parameter a in the 1 km spatial resolution model, $R^2 = 0.522$, RMSE = 0.123, bias = 0.107. Figure 5b shows the SEMP b of the cropland sites (Equation (14)):

$$b_{S30} = 0.4455 \times b_{S1000} + 0.0858 \quad (14)$$

where b_{S30} represents the parameter b in the 30 m spatial resolution model, b_{S1000} represents the parameter b in the 1 km spatial resolution model, $R^2 = 0.445$, RMSE = 0.211, and bias = −0.180. The results indicate that there is a strong scaling relation of model parameter a, and there is a strong scaling relation of model parameter b at the cropland sites. Figure 5c shows the SEMP a of the forest sites (Equation (15)):

$$a_{S30} = 0.5040 \times a_{S1000} + 0.3412 \quad (15)$$

where $R^2 = 0.768$, RMSE = 0.116, and bias = 0.062. Figure 5d shows the SEMP b of the forest sites (Equation (16)):

$$b_{S30} = 0.2353 \times b_{S1000} + 0.0794 \quad (16)$$

where $R^2 = 0.286$, RMSE = 0.199 and bias= −0.113. The results show that there is a strong scaling relation for parameter a in forest sites, and parameter b has a relatively lower R^2.

Generally, the scaling relation of NDVI-LAI models established at 30 m and 1 km spatial resolutions can be described by SEMPs. SEMPs describe the scaling relation of model parameters well for the cropland. SEMP a describes the scaling relation of the parameter a well for the forest, and SEMP b describes the scaling relation of the parameter b as relatively weak.

4.3. Accuracy of the Downscaled NDVI-LAI Statistical Model

The results and validation of the downscaled NDVI-LAI statistical model are analyzed in this section.

4.3.1. Cropland

For the Pshenichne site, the constructed model $F(P)$ at 1 km spatial resolution is shown in Equation (17), and the downscaled NDVI-LAI statistical model $f(p_{SD})$, which is suitable for 30 m spatial resolution, is shown in Equation (18):

$$NDVI_{S1000} = 0.508 LAI_{S1000}^{0.364} \quad (17)$$

$$NDVI_{S30} = 0.608 LAI_{S30}^{0.248} \quad (18)$$

In Figure 6a, the aquamarine curve represents the model $F(P)$, and the orange curve represents the downscaled model $f(p_{SD})$. The model $f(p)$, which is constructed directly with Landsat NDVI and field LAI, is shown in Equation (19):

$$NDVI_{S30} = 0.627 LAI_{S30}^{0.238} \quad (19)$$

The red curve in Figure 6a represents the model $f(p)$ at the Pshenichne site. The NDVI ratio (Equation (12)) between $f(p_{SD})$ and $f(p)$ is shown in Figure 6b.

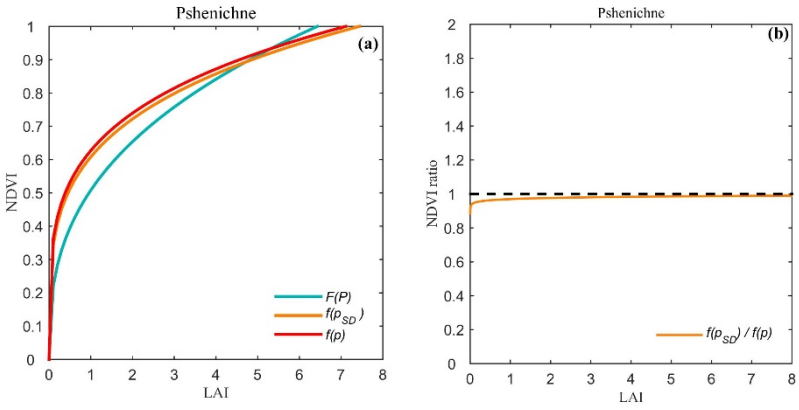

Figure 6. Results and validation of the downscaled model at the Pshenichne site. (**a**) The aquamarine curve is the model $F(P)$ at 1 km spatial resolution established by the Ordinary Least Squares (OLS) method; the orange curve is the downscaled model $f(p_{SD})$ established by SEMPs; the red curve is the model $f(p)$ at 30 m spatial resolution directly established by the OLS method; (**b**) the orange curve is the NDVI ratio between $f(p_{SD})$ and $f(p)$.

In Figure 6a, $f(p_{SD})$ is more similar to the model $f(p)$. In Figure 6b, the NDVI ratio between $f(P_{SD})$ and $f(p)$ ranges from 0.884 to 0.972 when the LAI ranges from 0.0001 to 8, and the ratio is close to 1. For the Pshenichne site, the accuracy of the downscaled model is high.

4.3.2. Forest

For the Camerons site, the model $F(P)$ at 1 km spatial resolution is shown in Equation (20), and the downscaled NDVI-LAI statistical model $f(p_{SD})$ is shown in Equation (21):

$$NDVI_{S1000} = 0.358LAI_{S1000}^{0.578} \quad (20)$$

$$NDVI_{S30} = 0.522LAI_{S30}^{0.215} \quad (21)$$

In Figure 7a, the aquamarine curve represents the model $F(P)$ and the orange curve represents the downscaled model $f(p_{SD})$. The model $f(p)$, which is constructed directly with Landsat NDVI and field LAI, is shown in Equation (22):

$$NDVI_{S30} = 0.563LAI_{S30}^{0.119} \quad (22)$$

The red curve in Figure 7a represents the model $f(p)$ at the Camerons site. The NDVI ratio between $f(p_{SD})$ and $f(p)$ is shown in Figure 7b.

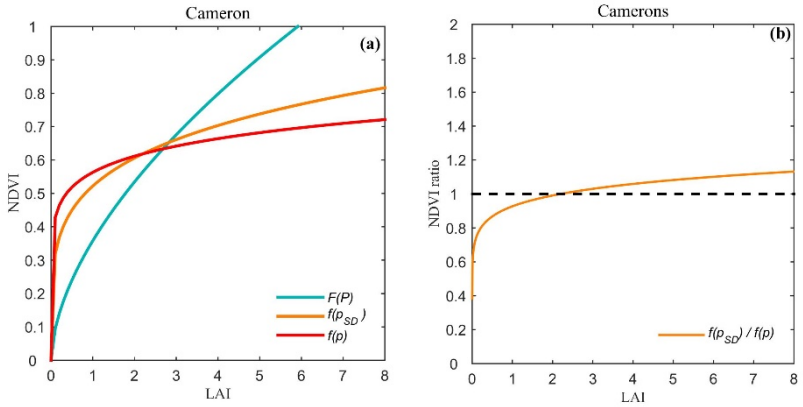

Figure 7. Results and evaluation of the downscaled model at the Camerons site. (**a**) The aquamarine curve is the model $F(P)$ at 1 km spatial resolution established by the OLS method; the orange curve is the downscaled model $f(p_{SD})$ established by SEMPs; the red curve is the model $f(p)$ at 30 m spatial resolution directly established by the OLS method; (**b**) the orange curve is the NDVI ratio between $f(p_{SD})$ and $f(p)$.

In Figure 7a, $f(p_{SD})$ is more similar to the model $f(p)$. In Figure 7b, the NDVI ratio between $f(p_{SD})$ and $f(p)$ ranges from 0.383 to 1.132 when the LAI ranges from 0.0001 to 8. When the LAI is greater than 1, the NDVI ratio is close to 1. For the Camerons site, the accuracy of the downscaled model is high**,** especially when the LAI value is greater than 1.

4.4. Accuracy of the Estimated Fine-resolution LAI

The results and validation of 30 m LAIs are analyzed in this section. Meanwhile, the comparison between the fine-resolution LAI estimated by the model-downscaling method and Ovakoglou's downscaling method [27] is shown in this section.

4.4.1. Crop

At the Pshenichne site, the field LAI data for LAI validation were distributed over 5 months and three years: May 2013, June and July 2014, and June and July 2015. The reference LAI map with 30 m spatial resolution in June 2015 was obtained from the ImagineS project.

The result evaluated by the ground LAI is shown in Figure 8a; RMSE = 0.821, and bias= 0.299. The result evaluated by the reference LAI map is shown in Figure 8b; RMSE = 0.573, and bias = 0.276. A scattering density map can analyze the distribution traits of data. When the dot density is larger, the color is closer to red; otherwise, the color is closer to blue. The scattering density map shows that the accuracy of the LAI maps with 30 m spatial resolutions based on the model-downscaling method is high.

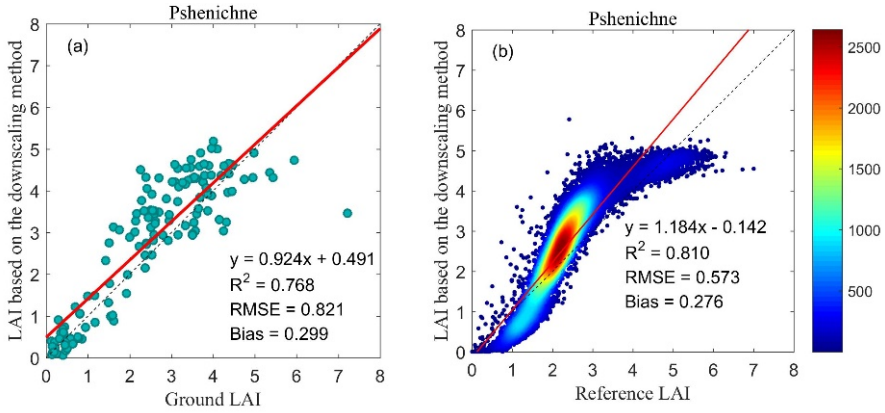

Figure 8. Evaluation of the fine-resolution LAI based on the model-downscaling method proposed in this paper at the Pshenichne site. (**a**) Ground LAI measurements; (**b**) the reference LAI map with 30 m spatial resolution obtained from the ImagineS project.

At the Pshenichne site, the LAI map produced by the model-downscaling method proposed in this paper is shown in Figure 9a; the LAI map produced by Ovakoglou's downscaling method [27] is shown in Figure 9b; the LAI map based on the model $F(P)$ is shown in Figure 9c. The reference LAI map obtained from the ImagineS project is shown in Figure 9d. The LAI map based on the model-downscaling method has a more similar spatial distribution to the reference LAI map and contains more detailed information than the reference LAI map. Comparing the LAI map in Figure 9a with the LAI map in Figure 9c, it is demonstrated that the model $F(P)$ records the vegetation characterization at the 1 km spatial resolution and the model $f(p_{SD})$ records the vegetation characterization at the 30 m spatial resolution. The model built at the coarse resolution is not suitable for fine-resolution LAI estimation.

Meanwhile, comparing the LAI map in Figure 9a with the LAI map in Figure 9b, the raster in Figure 9a has a more similar spatial distribution to the reference LAI map.

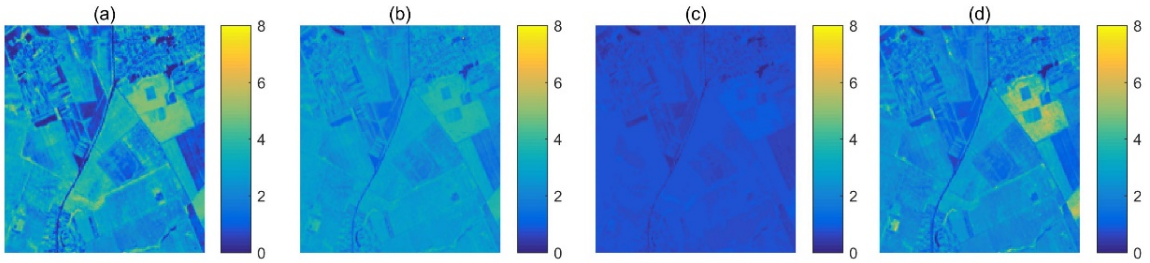

Figure 9. LAI maps with 30 m spatial resolution at the Pshenichne site. (**a**) Based on the model-downscaling method proposed in this paper; (**b**) based on Ovakoglou's downscaling method; (**c**) based on the model $F(P)$; (**d**) the reference LAI map with 30 m spatial resolution obtained from the ImagineS project.

The scattering density map between the LAI map in Figure 9a and the reference LAI map in Figure 9d is plotted in Figure 10a; RMSE = 0.573, and bias = 0.276. The scattering density map between the LAI map in Figure 9b and the reference LAI map in Figure 9d is plotted in Figure 10b; RMSE = 1.469, and bias = 0.293. The scattering density map between the LAI map in Figure 9c and the reference LAI map in Figure 9d is plotted in Figure 10c; RMSE = 1.700, and bias = −1.526. From Figure 10a–c, it is indicated that the LAI map based on the model-downscaling method has the highest accuracy. When considering the scaling effect of the model, the RMSE is smaller and the R^2 is higher.

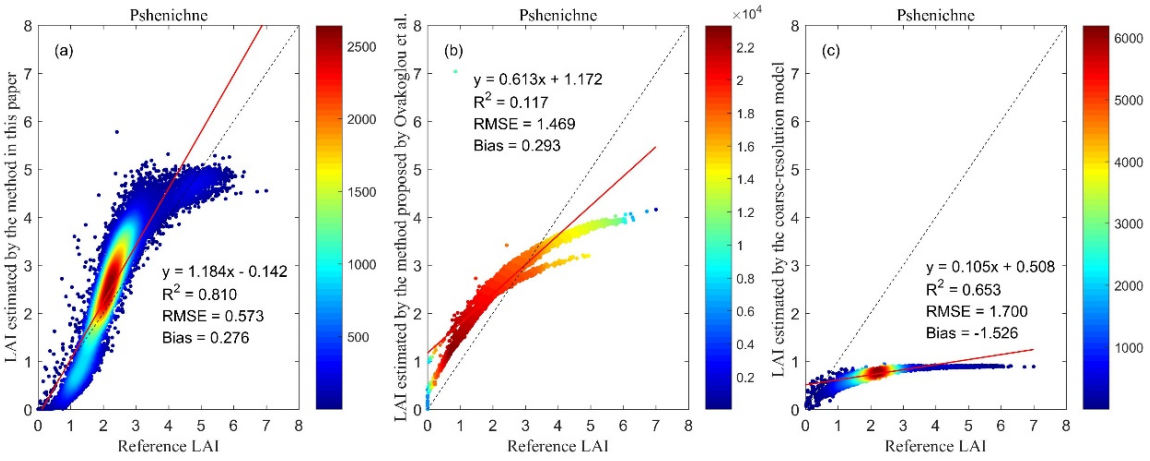

Figure 10. Scattering density map between the estimated LAI map and the reference LAI map at the Pshenichne site. (**a**) Based on the model-downscaling method proposed in this paper; (**b**) based on Ovakoglou's downscaling method; (**c**) based on the model $F(P)$.

4.4.2. Forest

For the Camerons site, the field LAI data for LAI validation were retrieved on March 3, 2004. The reference LAI map with 20 m spatial resolution on March 3, 2004 was obtained from the VALERI project. The reference LAI map was resampled to 30 m spatial resolution for LAI validation. The result evaluated by ground measurement data is shown in Figure 11a; RMSE = 0.515, and bias= 0.263. The result evaluated by the reference LAI map is shown in Figure 11b; RMSE = 0.523, and bias = −0.354. These results show that the accuracy of the LAI maps with 30 m spatial resolutions based on the model-downscaling method is high and can meet the application requirements for forests.

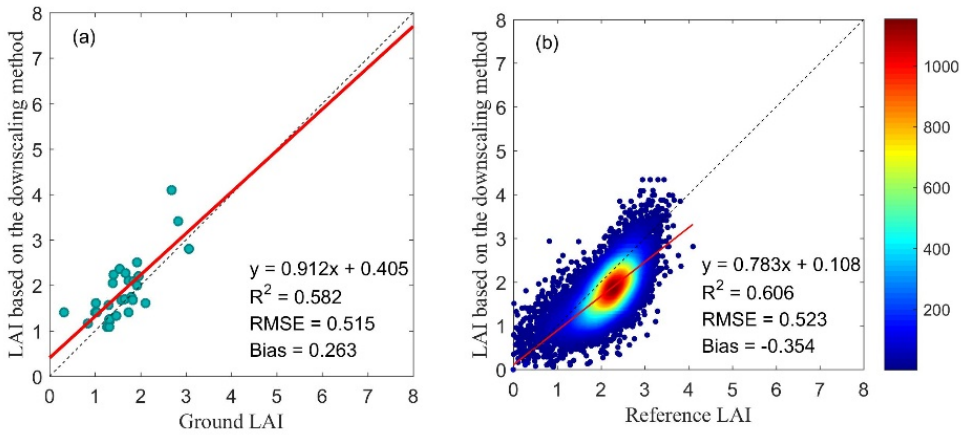

Figure 11. Evaluation of the fine-resolution LAI based on the model-downscaling method proposed in this paper at the Camerons site. (**a**) Ground LAI measurements. (**b**) Reference LAI map with 30 m spatial resolution obtained from the VAlidation of Land European Remote-Sensing Instruments (VALERI) project.

At the Camerons site, the LAI map based on the model-downscaling method proposed in this paper is shown in Figure 12a; the LAI map based on Ovakoglou's downscaling method [27] is shown in Figure 12b; the LAI map based on the model $F(P)$ is shown in Figure 12c. The reference LAI map obtained from the VALERI project is shown in Figure 12d. The LAI map produced by the model-downscaling method has a more similar spatial distribution to the reference LAI map and contains more detailed information than the reference LAI map. Comparing the LAI map in Figure 12a with the LAI map in Figure 12c, it is demonstrated that model $F(P)$ records the vegetation

characterization at the 1 km spatial resolution, and model $f(p_{SD})$ records the vegetation characterization at a 30 m spatial resolution. The model built at the coarse resolution is not suitable for fine-resolution LAI estimation.

Meanwhile, comparing the LAI map in Figure 12a with the LAI map in Figure 12b, the raster in Figure 12a has a more similar spatial distribution to the reference LAI map.

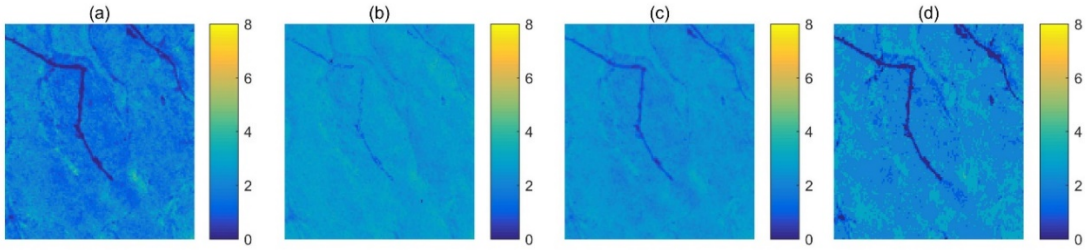

Figure 12. LAI maps with 30 m spatial resolutions at the Camerons site. (**a**) Based on the model-downscaling method proposed in this paper; (**b**) based on Ovakoglou's downscaling method; (**c**) based on the model $F(P)$; (**d**) the reference LAI map with 30 m spatial resolution obtained from the VALERI project.

The scattering density map between the LAI map in Figure 12a and the reference LAI map in Figure 12d is plotted in Figure 13a; RMSE = 0.523, and bias = −0.354. The scattering density map between the LAI map in Figure 12b and the reference LAI map in Figure 12d is plotted in Figure 13b; RMSE = 0.612, and bias = 0.437. The scattering density map between the LAI map in Figure 12c and the reference LAI map in Figure 12d is plotted in Figure 13c; RMSE = 0.385, and bias = 0.187. From Figure 13a–c, it is indicated that the R^2 of the estimated LAI in Figure 13a is similar to the estimated LAI in Figure 13b,c. In Figure 7a, there is little difference between the downscaled model and the coarse-resolution model when the LAI is around 2.5, and the LAI values are mostly around 2.5 at this site. Therefore, the RMSEs in Figure 13a,c are similar.

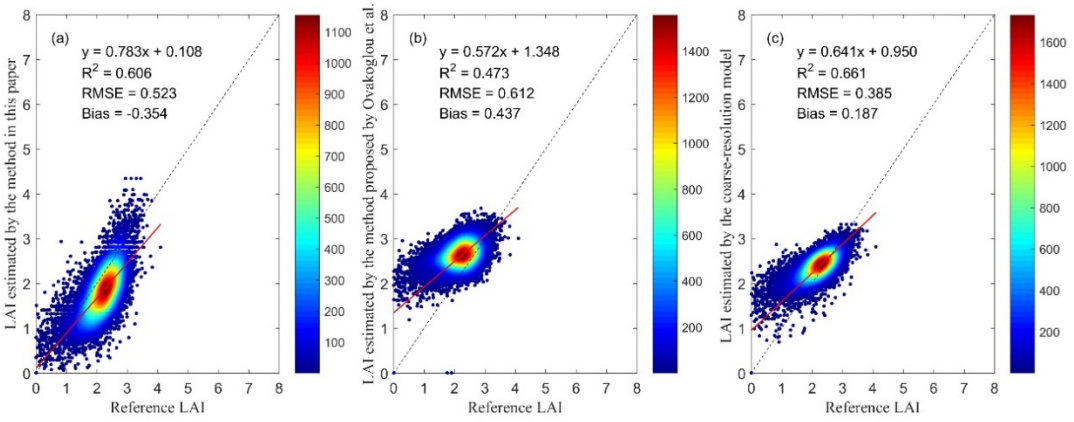

Figure 13. Scattering density map between the estimated LAI map and the reference LAI map at the Camerons site. (**a**) Based on the downscaling method proposed in this paper; (**b**) based on Ovakoglou's downscaling method; (**c**) based on the model $F(P)$.

Overall, the LAIs estimated with 30 m spatial resolutions based on the model-downscaling method in this paper have high accuracy, and this model-downscaling method is viable. Moreover, the scaling effect of the model should be considered in multiscale LAI estimation.

5. Discussion

5.1. Feasibility of the Model-Downscaling Method

We proposed a model-downscaling method for fine-resolution LAI estimation. This method was tested by a nonlinear statistical model form of the NDVI and LAI. The results showed the viability of this model-downscaling method. This method has two characteristics: first, as the model form is invariant at different spatial resolutions, it is easy to apply to other models, and it has the potential to be extended to physical models; second, it is convenient to select model parameters that are sensitive to the spatial resolution, and we can establish SEMPs for the sensitive parameters of the model. From the perspective of modeling, this model-downscaling method is flexible and easy to apply.

Existing results have also indicated some problems that need to be further studied and solved.

First, the model form must be considered to ensure high model accuracy [43,44], as it provides the basic data for the SEMPs; for example, the semiempirical model form (Equation (23)) [38] is chosen for the model-downscaling method:

$$NDVI = NDVI_{\infty} - (NDVI_{\infty} - NDVI_{g}) \times e^{-k \times LAI} \quad (23)$$

where $NDVI_{\infty}$ represents the maximum NDVI, $NDVI_{g}$ represents the NDVI value of soil, and k represents the relative change in the NDVI when the LAI changes, which is equivalent to the extinction coefficient. We tried to use a semiempirical model form to construct the SEMPs. Figure 14 shows the results of model construction.

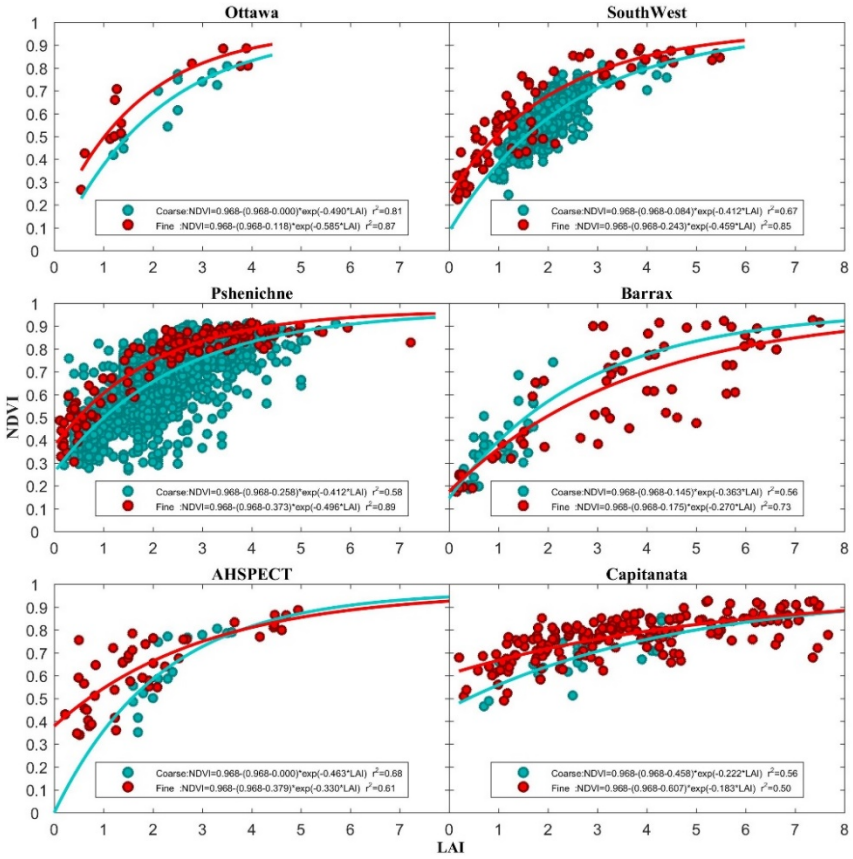

Figure 14. Semiempirical NDVI-LAI statistical model established at the two spatial resolutions (30 m and 1 km spatial resolutions) and at the six cropland sites. The red points represent the (LAI, NDVI) datasets with 30 m spatial resolutions, and the red curves represent the models $f(p)$ at 30 m spatial resolutions; the aquamarine points represent the (LAI, NDVI) datasets with 1 km spatial resolutions, and the aquamarine curves represent the models $F(P)$ at 1 km spatial resolutions.

Comparing the models shown in Figure 14 with the models shown in Figure 3, the model accuracy slightly improved at most sites. In the process of SEMP construction, we found that the $NDVI_\infty$ values hardly change with the spatial resolution. It is not necessary to establish a SEMP for all the model parameters. In this paper, we set $NDVI_\infty$ to 0.986 because the mean value of $NDVI_\infty$ values at the six cropland sites and the two spatial resolutions is 0.986. The scaling equations of k and $NDVI_g$ are shown in Figure 15.

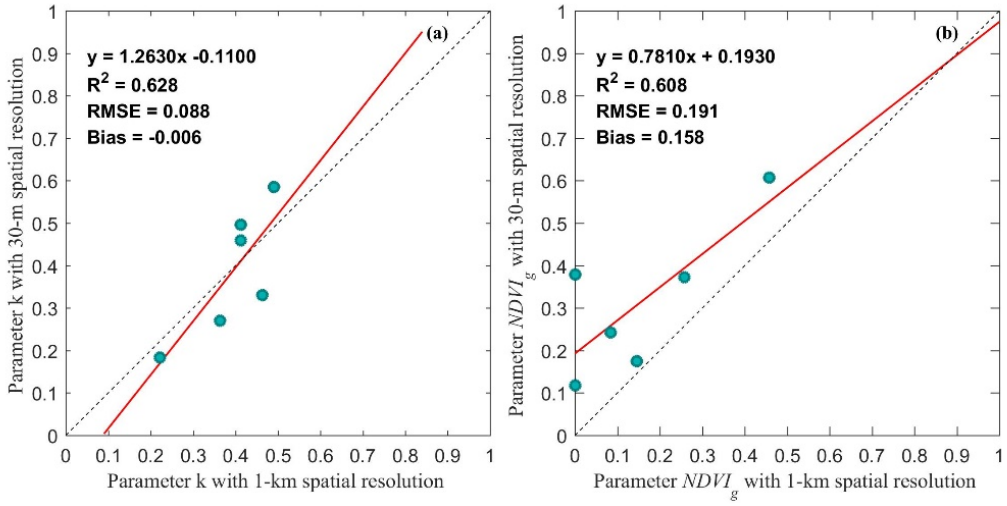

Figure 15. The scaling equations of model parameters at the cropland sites. (**a**) k; (**b**) $NDVI_g$.

In Figure 15, the R^2 of SEMP k is 0.628, and the R^2 of SEMP $NDVI_g$ is 0.608. Parameter k changes slightly with spatial resolutions, and parameter $NDVI_g$ changes with spatial resolutions. Moreover, compared with the SEMPs based on Equation (4), in which the R^2 of the SEMP a is 0.522 and the R^2 of the SEMP b is 0.445, the SEMPs based on Equation (23) show higher R^2 values.

Therefore, the model form affects the accuracy of the SEMP, and we need to identify the sensitive parameters of a specific model form. In the future, we will try to replace statistical models with physical models, select scale-sensitive parameters and establish SEMPs.

5.2. The Amount of Data Needed for the Statistical Model

The accuracy of a statistical model depends on the amount of modelling data [45]. Currently, in this paper, there are two types of statistical models: the NDVI-LAI model and the SEMPs. The amount of ground LAI data retrieved from the cropland sites is large, and the uncertainty in the NDVI-LAI model is low, but at the forest sites, the amount of ground data is limited, and the uncertainty in the NDVI-LAI model is higher. In this paper, the number of selected global sites is limited, so the data amount of the model parameter dataset influences the accuracy of the SEMPs.

It is difficult to obtain the reference value of the LAI at different spatial resolutions, which affects the study of the scale issue, but our research is based on the actual needs of LAI and proposes a possible downscaling scheme to support the application under the condition that there is not enough fine-resolution ground LAI measurement data to build an NDVI-LAI statistical model with high accuracy; therefore, the method in this paper has reference value.

6. Conclusions

We proposed a model-downscaling method based on scaling equations of model parameters (SEMPs) for fine-resolution LAI estimation by considering the scaling effect of the model. LAI and

NDVI data at 1 km and 30 m at six crop sites and eight forest sites were collected. Three steps were included in this method. The first step was the construction of SEMPs. NDVI-LAI statistical models were built at 1 km and 30 m spatial resolutions. The SEMPs were built using the parameter datasets of the models at 30 m and 1 km spatial resolutions for cropland and forest, respectively. The second step was the establishment of the downscaled NDVI-LAI statistical model based on SEMPs and $F(P)$ at a validation site. The achieved downscaled model records the land surface information at 30 m spatial resolution at the validation site. The third step was inputting the Landsat NDVI into the downscaled model to estimate the 30 m LAI at the validation site. The Pshenichne crop site and Camerons forest site were chosen to validate the proposed method. The validation results show that at the crop site, the RMSE is 0.821 and the bias is 0.299 when compared with the ground LAI. The RMSE is 0.573 and the bias is 0.276 when compared with the referenced LAI map. At the forest site, the RMSE is 0.515 and 0.523, and the bias is 0.263 and −0.354 when compared with ground LAI and the referenced LAI map, respectively. The results are better than those of Ovakoglou's downscaling method. The spatial distribution of the fine-resolution LAI based on this model-downscaling method is more similar to the reference fine-resolution LAI maps and contains more detailed information than the reference LAI.

In conclusion, the results of this study demonstrate that a scaling relation of the remote-sensing model exists, and scaling equations of model parameters can achieve model scaling of models at different spatial resolutions. The basic framework of this model-downscaling method is referable and viable for fine-resolution LAI estimation. Further verification of this method requires more data and experiments.

Author Contributions: J.W. and J.Z. proposed the ideas; J.W., J.Z., and H.Z. (Helin Zhang) preprocessed and analyzed the data; J.W., J.Z., H.Z. (Hongmin Zhou), and R.S. prepared the paper. All authors have read and agreed to the published version of the manuscript.

Funding: This research was funded by the National Natural Science Foundation of China under grant 41801242; the Chinese 973 Program, grant number 2013CB733403; the National Key R&D Program of China (2016YFB0501502).

Acknowledgments: We thank professor Zhiqiang Xiao provide the GLASS LAI product for us. We also thank USGS EarthExplorer, Earthdata, VALERI and ImagineS who made the global LAI products and validation data available.

Conflicts of Interest: The authors declare no conflict of interest.

References

1. Chen, J.M.; Black, T.A. Defining leaf area index for non-flat leaves. *Plant Cell Environ.* **1992**, *15*, 421–429, doi:10.1111/j.1365-3040.1992.tb00992.x.
2. Ganopolski, A.; Kubatzki, C.; Claussen, M.; Brovkin, V.; Petoukhov, V. The influence of vegetation-atmosphere-ocean interaction on climate during the mid-Holocene. *Science* **1998**, *280*, 1916–1919, doi:10.1126/science.280.5371.1916.
3. Myneni, R.B.; Hoffman, S.; Knyazikhin, Y.; Privette, J.L.; Glassy, J.; Tian, Y.; Wang, Y.; Song, X.; Zhang, Y.; Smith, G.R.; et al. Global products of vegetation leaf area and fraction absorbed PAR from year one of MODIS data. *Remote Sens. Environ.* **2002**, *83*, 214–231, doi:10.1016/s0034-4257(02)00074-3.
4. Verger, A.; Baret, F.; Weiss, M. GEOV2/VGT: Near real time estimation of global biophysical variables from VEGETATION-P data. In Proceedings of the 7th International Workshop on the Analysis of Multi-Temporal Remote Sensing Images, Banff, AB, Canada, 25–27 June 2013; pp. 1–4.
5. Baret, F.; Weiss, M.; Lacaze, R.; Camacho, F.; Makhmara, H.; Pacholcyzk, P.; Smets, B. GEOV1: LAI and FAPAR essential climate variables and FCOVER global time series capitalizing over existing products. Part1: Principles of development and production. *Remote Sens. Environ.* **2013**, *137*, 299–309, doi:10.1016/j.rse.2012.12.027.
6. Xiao, Z.Q.; Liang, S.L.; Wang, J.D.; Chen, P.; Yin, X.J.; Zhang, L.Q.; Song, J.L. Use of General Regression Neural Networks for Generating the GLASS Leaf Area Index Product From Time-Series MODIS Surface Reflectance. *IEEE Trans. Geosci. Remote Sens.* **2014**, *52*, 209–223, doi:10.1109/tgrs.2013.2237780.

7. Yan, K.; Park, T.; Chen, C.; Xu, B.D.; Song, W.J.; Yang, B.; Zeng, Y.L.; Liu, Z.; Yan, G.J.; Knyazikhin, Y.; et al. Generating Global Products of LAI and FPAR From SNPP-VIIRS Data: Theoretical Background and Implementation. *IEEE Trans. Geosci. Remote Sens.* **2018**, *56*, 2119–2137, doi:10.1109/tgrs.2017.2775247.
8. Garcia-Haro, F.J.; Campos-Taberner, M.; Munoz-Mari, J.; Laparra, V.; Camacho, F.; Sanchez-Zapero, J.; Camps-Valls, G. Derivation of global vegetation biophysical parameters from EUMETSAT Polar System. *ISPRS J. Photogramm. Remote Sens.* **2018**, *139*, 57–74, doi:10.1016/j.isprsjprs.2018.03.005.
9. Fang, H.L.; Zhang, Y.H.; Wei, S.S.; Li, W.J.; Ye, Y.C.; Sun, T.; Liu, W.W. Validation of global moderate resolution leaf area index (LAI) products over croplands in northeastern China. *Remote Sens. Environ.* **2019**, *233*, 19, doi:10.1016/j.rse.2019.111377.
10. Qu, Y.H.; Zhang, Y.Z.; Xue, H.Z. Retrieval of 30-m-Resolution Leaf Area Index From China HJ-1 CCD Data and MODIS Products Through a Dynamic Bayesian Network. *IEEE J. Sel. Top. Appl. Earth Obs. Remote Sens.* **2014**, *7*, 222–228, doi:10.1109/jstars.2013.2259472.
11. Jin, H.A.; Li, A.N.; Yin, G.F.; Xiao, Z.Q.; Bian, J.H.; Nan, X.; Jing, J.C. A Multiscale Assimilation Approach to Improve Fine-Resolution Leaf Area Index Dynamics. *IEEE Trans. Geosci. Remote Sens.* **2019**, *57*, 8153–8168, doi:10.1109/tgrs.2019.2918548.
12. Yin, G.F.; Li, A.N.; Zeng, Y.L.; Xu, B.D.; Zhao, W.; Nan, X.; Jin, H.A.; Bian, J.H. A Cost-Constrained Sampling Strategy in Support of LAI Product Validation in Mountainous Areas. *Remote Sens.* **2016**, *8*, 704, doi:10.3390/rs8090704.
13. Zhai, H.; Huang, F.; Qi, H. Generating High Resolution LAI Based on a Modified FSDAF Model. *Remote Sens.* **2020**, *12*, 150, doi:10.3390/rs12010150.
14. Liang, S. *Quantitative Remote Sensing of Land Surfaces*; China Science Publishing & Media Ltd.: Beijing, China, 2012; p. 326.
15. Atkinson, P.M. Downscaling in remote sensing. *Int. J. Appl. Earth Obs. Geoinf.* **2013**, *22*, 106–114, doi:10.1016/j.jag.2012.04.012.
16. Chen, J.M. Spatial scaling of a remotely sensed surface parameter by contexture. *Remote Sens. Environ.* **1999**, *69*, 30–42, doi:10.1016/s0034-4257(99)00006-1.
17. Hu, Z.L.; Islam, S. A framework for analyzing and designing scale invariant remote sensing algorithms. *IEEE Trans. Geosci. Remote Sens.* **1997**, *35*, 747–755, doi:10.1109/36.581996.
18. Liang, S. Numerical experiments on the spatial scaling of land surface albedo and leaf area index. *Remote Sens. Rev.* **2000**, *19*, 225–242, doi:10.1080/02757250009532420.
19. Wu, H.; Tang, B.H.; Li, Z.L. Impact of nonlinearity and discontinuity on the spatial scaling effects of the leaf area index retrieved from remotely sensed data. *Int. J. Remote Sens.* **2013**, *34*, 3503–3519, doi:10.1080/01431161.2012.716537.
20. Wu, H.; Li, Z.L. Scale Issues in Remote Sensing: A Review on Analysis, Processing and Modeling. *Sensors* **2009**, *9*, 1768–1793, doi:10.3390/s90301768.
21. Jiang, J.L.; Ji, X.S.; Yao, X.; Tian, Y.C.; Zhu, Y.; Cao, W.X.; Cheng, T. Evaluation of Three Techniques for Correcting the Spatial Scaling Bias of Leaf Area Index. *Remote Sens.* **2018**, *10*, 221, doi:10.3390/rs10020221.
22. Garrigues, S.; Allard, D.; Baret, F.; Weiss, M. Influence of landscape spatial heterogeneity on the non-linear estimation of leaf area index from moderate spatial resolution remote sensing data. *Remote Sens. Environ.* **2006**, *105*, 286–298, doi:10.1016/j.rse.2006.07.013.
23. Jiang, J.L.; Liu, X.N.; Liu, C.H.; Wu, L.; Xia, X.P.; Liu, M.L.; Du, Z.H. Analyzing the Spatial Scaling Bias of Rice Leaf Area Index from Hyperspectral Data Using Wavelet-Fractal Technique. *IEEE J. Sel. Top. Appl. Earth Obs. Remote Sens.* **2015**, *8*, 3068–3080, doi:10.1109/jstars.2014.2346251.
24. Wu, L.; Qin, Q.M.; Liu, X.N.; Ren, H.Z.; Wang, J.H.; Zheng, X.P.; Ye, X.; Sun, Y.J. Spatial Up-Scaling Correction for Leaf Area Index Based on the Fractal Theory. *Remote Sens.* **2016**, *8*, 197, doi:10.3390/rs8030197.
25. Gao, F.; Anderson, M.C.; Kustas, W.P.; Wang, Y.J. Simple method for retrieving leaf area index from Landsat using MODIS leaf area index products as reference. *J. Appl. Remote Sens.* **2012**, *6*, 063554, doi:10.1117/1.Jrs.6.063554.
26. Yu, T.; Sun, R.; Xiao, Z.Q.; Zhang, Q.; Wang, J.M.; Liu, G. Generation of High Resolution Vegetation Productivity from a Downscaling Method. *Remote Sens.* **2018**, *10*, 748, doi:10.3390/rs10111748.
27. Ovakoglou, G.; Alexandridis, T.K.; Clevers, J.G.P.W.; Gitas, I.Z. Downscaling of MODIS leaf area index using landsat vegetation index. *Geocarto Int.* **2020**, in press, doi:10.1080/10106049.2020.1750062.

28. Tian, Y.H.; Wang, Y.J.; Zhang, Y.; Knyazikhin, Y.; Bogaert, J.; Myneni, R.B. Radiative transfer based scaling of LAI retrievals from reflectance data of different resolutions. *Remote Sens. Environ.* **2003**, *84*, 143–159, doi:10.1016/s0034-4257(02)00102-5.
29. Zhang, X.; Yan, G.; Li, Q.; Li, Z.L.; Wan, H.; Guo, L. Evaluating the fraction of vegetation cover based on NDVI spatial scale correction model. *Int. J. Remote Sens.* **2006**, *27*, 5359–5372, doi:10.1080/01431160600658107.
30. Jacquemoud, S.; Baret, F.; Andrieu, B.; Danson, F.M.; Jaggard, K. Extraction of vegetation biophysical parameters by inversion of the prospect plus sail models on sugar-beet canopy reflectance data—Application to tm and aviris sensors. *Remote Sens. Environ.* **1995**, *52*, 163–172, doi:10.1016/0034-4257(95)00018-v.
31. Li, X.W.; Strahler, A.H. Geometric-Optical Bidirectional Reflectance Modeling of the Discrete Crown Vegetation Canopy—Effect of Crown Shape And Mutual Shadowing. *IEEE Trans. Geosci. Remote Sens.* **1992**, *30*, 276–292, doi:10.1109/36.134078.
32. Friedl, M.A.; Davis, F.W.; Michaelsen, J.; Moritz, M.A. Scaling and uncertainty in the relationship between the NDVI and land surface biophysical variables: An analysis using a scene simulation model and data from FIFE. *Remote Sens. Environ.* **1995**, *54*, 233–246, doi:10.1016/0034-4257(95)00156-5.
33. Asrar, G.; Myneni, R.B.; Choudhury, B.J. Spatial heterogeneity in vegetation canopies and remote sensing of absorbed photosynthetically active radiation: A modeling study. *Remote Sens. Environ.* **1992**, *41*, 85–103, doi:10.1016/0034-4257(92)90070-z.
34. Li, X.W.; Wang, J.D.; Strahler, A.H. Scale effect of Planck's law over nonisothermal blackbody surface. *Sci. China Ser. E Technol. Sci.* **1999**, *42*, 652–656, doi:10.1007/bf02917003.
35. Baret, F.; Weiss, M.; Allard, D.; Garrigue, S.; Leroy, M.; Jeanjean, H.; Fernandes, R.; Myneni, R.; Privette, J.; Bohbot, H.; et al. VALERI: A network of sites and methodology for the validation of medium spatial resolution land products. *Remote Sens. Environ.* **2005**, *76*, 36–39.
36. Pisek, J.; Chen, J.M.; Lacaze, R.; Sonnentag, O.; Alikas, K. Expanding global mapping of the foliage clumping index with multi-angular POLDER three measurements: Evaluation and topographic compensation. *ISPRS J. Photogramm. Remote Sens.* **2010**, *65*, 341–346, doi:10.1016/j.isprsjprs.2010.03.002.
37. Kang, Y.H.; Ozdogan, M.; Zipper, S.C.; Roman, M.O.; Walker, J.; Hong, S.Y.; Marshall, M.; Magliulo, V.; Moreno, J.; Alonso, L.; et al. How Universal Is the Relationship between Remotely Sensed Vegetation Indices and Crop Leaf Area Index? A Global Assessment. *Remote Sens.* **2016**, *8*, 597, doi:10.3390/rs8070597.
38. Liu, J.G.; Pattey, E.; Jego, G. Assessment of vegetation indices for regional crop green LAI estimation from Landsat images over multiple growing seasons. *Remote Sens. Environ.* **2012**, *123*, 347–358, doi:10.1016/j.rse.2012.04.002.
39. Carlson, T.N.; Ripley, D.A. On the relation between NDVI, fractional vegetation cover, and leaf area index. *Remote Sens. Environ.* **1997**, *62*, 241–252, doi:10.1016/s0034-4257(97)00104-1.
40. Qiao, K.; Zhu, W.Q.; Xie, Z.Y.; Li, P.X. Estimating the Seasonal Dynamics of the Leaf Area Index Using Piecewise LAI-VI Relationships Based on Phenophases. *Remote Sens.* **2019**, *11*, 689, doi:10.3390/rs11060689.
41. Kobayashi, H.; Suzuki, R.; Kobayashi, S. Reflectance seasonality and its relation to the canopy leaf area index in an eastern Siberian larch forest: Multi-satellite data and radiative transfer analyses. *Remote Sens. Environ.* **2007**, *106*, 238–252, doi:10.1016/j.rse.2006.08.011.
42. Birky, A.K. NDVI and a simple model of deciduous forest seasonal dynamics. *Ecol. Model.* **2001**, *143*, 43–58, doi:10.1016/s0304-3800(01)00354-4.
43. Chen, J.M.; Cihlar, J. Retrieving leaf area index of boreal conifer forests using landsat TM images. *Remote Sens. Environ.* **1996**, *55*, 153–162, doi:10.1016/0034-4257(95)00195-6.
44. Turner, D.P.; Cohen, W.B.; Kennedy, R.E.; Fassnacht, K.S.; Briggs, J.M. Relationships between leaf area index and Landsat TM spectral vegetation indices across three temperate zone sites. *Remote Sens. Environ.* **1999**, *70*, 52–68, doi:10.1016/s0034-4257(99)00057-7.
45. Shi, Y.C.; Wang, J.D.; Wang, J.; Qu, Y.H. A Prior Knowledge-Based Method to Derivate High-Resolution Leaf Area Index Maps with Limited Field Measurements. *Remote Sens.* **2017**, *9*, 13, doi:10.3390/rs9010013.

Publisher's Note: MDPI stays neutral with regard to jurisdictional claims in published maps and institutional affiliations.

© 2020 by the authors. Licensee MDPI, Basel, Switzerland. This article is an open access article distributed under the terms and conditions of the Creative Commons Attribution (CC BY) license (http://creativecommons.org/licenses/by/4.0/).